Smart Structures and Systems, *Vol. 23, No. 5 (2019) 405-420*
DOI: https://doi.org/10.12989/sss.2019.23.5.405

Vibration characteristics of offshore wind turbine tower with gravity-based foundation under wave excitation

Cong-Uy Nguyen[a], So-Young Lee[b], Thanh-Canh Huynh[c], Heon-Tae Kim[d] and Jeong-Tae Kim*

Department of Ocean Engineering, Pukyong National University, 45 Yongso-ro, Nam-gu, Busan 48513, Republic of Korea

(Received January 9, 2019, Revised April 22, 2019, Accepted April 24, 2019)

Abstract. In this study, vibration characteristics of offshore wind turbine tower (WTT) with gravity-based foundation (GBF) are identified from dynamic responses under wave-induced excitations. The following approaches are implemented to achieve the objective. Firstly, the operational modal analysis methods such as frequency domain decomposition (FDD) and stochastic subspace identification (SSI) are selected to estimate modal parameters from output-only dynamic responses. Secondly, a GBF WTT model composed of superstructure, substructure and foundation is simulated as a case study by using a structural analysis program, MIDAS FEA. Thirdly, wave pressures acting on the WTT structure are established by nonlinear regular waves which are simulated from a computational fluid software, Flow 3D. Wave-induced acceleration responses of the target structure are analyzed by applying the simulated wave pressures to the GBF WTT model. Finally, modal parameters such as natural frequencies and mode shapes are estimated from the output-only acceleration responses and compared with the results from free vibration analysis. The effect of wave height and period on modal parameter extraction is also investigated for the mode identification of the GBF WTT.

Keywords: wind turbine tower; caisson foundation; vibration characteristics; wave excitation

1. Introduction

The demand for clean energy increases due to the environmental issue around the world. It is reported that the electricity generation from the wind energy covers 11.6% of the EU total electricity demand in 2017 (Wind EUROPE 2018) while the Korean government plans to generate 20% of total renewable energy from wind energy in 2030 (MOTIE 2018). Wind energy can be generated in large scale from offshore wind farm since there is high potential of wind power along the coastal line. The offshore wind turbine towers are often classified based on their support types such as pile, jacket, suction bucket, floating mooring, and gravity-based caisson (Nguyen *et al.* 2017, Wang *et al.* 2018). Among those types, the gravity-based caisson foundation becomes popular thanks to simple design, fast installation and cost efficiency (Chong and Li 2016, 4Coffshore 2018).

For the safety of the wind turbine tower (WTT) with gravity-based foundation (GBF), it is important to understand dynamic characteristics of the integrated system which includes wind turbine tower, caisson and foundation bed (Smaling 2014, Esteban *et al*. 2015, Risi *et al.* 2018, Banerjee *et al.* 2018). The tower consists of segmental slender columns fastened by bolted flanges and a rotor operating nacelle on its top. The foundation includes a caisson and a gravel mound layer on the seabed, which support the tower. During the lifetime, the GBF WTT is exposed to extreme conditions like storm surge, earthquake, typhoons or even light striking. Regarding to structural damage, the worst scenario is that those extreme loading conditions are mixed with the inborn behaviors of the GBF WTT such as heavy self-weight and blade rotation-induced dynamic loading (Damgaard 2014, Petersen *et al.* 2015, Wang *et al.* 2017). The slender vertical tower can be damaged as similar as local buckling, crack or bolt-loosening in segmental joints. The self-load may create the settlement of the seabed, and the severe wave condition may cause local scouring in the caisson foundation. The above-mentioned damage in tower and foundation leads to the change of structural properties including boundary conditions and consequently results in the change of vibration characteristics (Lee and Kim 2015, Nguyen *et al*. 2017, 2018, Wichramasinghe *et al*. 2018).

Considering the fact that the substructure of the GBF WTT is submerged, an important question is how to monitor dynamic responses that can represent the vibration characteristics of the entire system. At least two technical issues should be solved to answer the question. The first issue is the limited accessibility of the substructure of the GBF WTT due to the submerged condition. Under the limited circumstance, dynamic responses can be locally measured from the tower. Then there is a need to interpret the tower’s responses that contain the information of a whole structural system including the submerged caisson and foundation properties (Huynh *et al.* 2018). The second issue is the limitation of excitation source for sufficient

*Corresponding author, Professor
E-mail: idis@pknu.ac.kr
[a] Graduate Student
[b] Post-doctoral Researcher
[c] Post-doctoral Researcher
[d] Professor

ISSN: 1738-1584 (Print), 1738-1991 (Online)

modal parameter extraction. The change of vibration characteristics due to the structural damage in tower and foundation should be identified from in-field measurement of wave-induced dynamic responses of the WTT above sea level (Lee *et al*. 2018).

Until now, the feasibility of monitoring vibration features (e.g., natural frequency and mode shape) from measuring wave-induced dynamic responses has not been evaluated for the GBF WTT. The so-called output-only modal analysis methods can be adopted in cooperated with the measurement of wave-induced dynamic responses to estimate the vibration characteristics of the GBF WTT under the above-mentioned conditions (Yi *et al.* 2004, Lee *et al.* 2013, 2015). Upon noticing the relative motions of the subsystems (e.g., flexible tower, rigid caisson, and deformable foundation mound and seabed), the vibration characteristics of the tower-caisson-foundation system can be decoded from the interacted modal responses of the free vibration analysis (Lee *et al*. 2018).

In this study, vibration characteristics of a GBF WTT model are identified from wave-induced dynamic responses by the combined use of the output-only modal analysis and the free vibration analysis. The following approaches are implemented to achieve the objective. Firstly, an output-only modal analysis approach which combines the stochastic subspace identification method and the frequency-domain decomposition method is designed to estimate modal parameters from wave-induced ambient vibration signals. Secondly, a GBF WTT model composed of superstructure, substructure and foundation is simulated by using a structural analysis program, MIDAS FEA. A 3.0 MW offshore wind turbine with a caisson foundation is simulated as the target structure for the numerical modeling. Thirdly, acceleration responses of the target structure are analyzed by applying wave excitations to the GBF WTT model. Dynamic wave pressures are established as the wave excitations by simulating nonlinear regular waves from a computational fluid software, Flow 3D. Finally, the output-only modal analysis approach is used to estimate modal parameters (i.e., natural frequencies and mode shapes) from the wave-induced acceleration responses and compared with the results obtained from the free vibration analysis. The effect of wave height and period on modal parameter extraction is also investigated for the mode identification of the GBF WTT.

2. Vibration analysis method for GBF WTT under wave excitation

2.1 Vibration monitoring condition of GBF WTT

Vibration monitoring of the GBF WTT is limited with respect to sensor placement and excitation source. Since the caisson foundation is submerged under sea water, being subjected to buoyancy, hydrostatic pressure and wave force, only the tower is accessible for vibration measurement. The wave-induced excitation on the rigid caisson, which is placed between the flexible tower and the deformable foundation including rubble mound and sea bed, produces integrated vibration responses of the entire structural system.

A structural system is represented by structural dynamic characteristics such as stiffness, mass, and damping properties. Its acceleration responses depend on the structural characteristics and it can be defined as

$$\ddot{\boldsymbol{u}}_t = [\mathrm{M}]^{-1}(\{F\} - \dot{\boldsymbol{u}}_t[\mathrm{C}] - \boldsymbol{u}_t[\mathrm{K}]) \tag{1}$$

in which $\boldsymbol{u}_t$, $\dot{\boldsymbol{u}}_t$ and $\ddot{\boldsymbol{u}}_t$ represent the displacement, velocity, and acceleration vectors, respectively; [M], [K] and [C] represent the mass matrix, stiffness matrix, and damping matrix, respectively; and $\{F\}$ is the vector of external wave forces.

The acceleration response provides information of the dynamic structural parameters that may be feasible for structural integrity assessment. In field practice, it is very hard to estimate the input wave load $\{F\}$ acting on the target structure, so that the available information, in most cases, is limited as the output vibration response (e.g., acceleration signal $\{\ddot{u}\}$ of the wind turbine tower). For the forced response of a damped structural system, the general receptance frequency response function (FRF) can be simplified in a complex form as follows (Ewins 2000)

$$\mathrm{FRF}(\omega) = ([\mathrm{K}] + i\omega[\mathrm{C}] - \omega^2[\mathrm{M}])^{-1} \tag{2}$$

in which the FRF is defined as a force to displacement response ratio in a frequency domain. As Eq. (1) can be equivalently interpreted as Eq. (2), the system's dynamic characteristics can be estimated via modal parameters such as natural frequency, modal damping and mode shape.

2.2 Output-only modal analysis methods

For an ambient condition like stochastic random excitation, the system's acceleration signals are output-only (i.e., unknown input force) vibration responses. To extract modal parameters from output-only vibration responses, modal analysis can be performed in time-domain or frequency-domain. In this study, combined time-domain and frequency-domain methods were selected to estimate modal parameters such as natural frequency, modal damping and mode shape of the GBF WTT. As the time-domain method, we selected the stochastic subspace identification (SSI) method (Overschee and De Moor 1996). As the frequency-domain method, we also selected the frequency domain decomposition (FDD) method (Brinker *et al.* 2000). According to a comparative study by Yi and Yun (2004), those two methods showed good performances in terms of accuracy, the computational time and simplicity.

2.2.1 Frequency-domain decomposition method

The frequency domain decomposition (FDD) method is a technique that decomposes the spectral density function matrix and generates a set of single degree of freedom systems from the response (Brinker *et al.* 2000). The procedure of the FDD method is summarized as follows Park (2009):

In Step 1, a set of output responses from n sensors on a structure is acquired. In Step 2, the power spectral density (PSD) matrix is calculated as follows

$$\boldsymbol{S}_{yy}(\omega) = \begin{bmatrix} S_{11}(\omega) & S_{21}(\omega) & \cdots & S_{1n}(\omega) \\ S_{21}(\omega) & S_{22}(\omega) & & S_{2n}(\omega) \\ \vdots & & \ddots & \vdots \\ S_{n1}(\omega) & S_{n2}(\omega) & \cdots & S_{nn}(\omega) \end{bmatrix} \quad (3)$$

where the $\boldsymbol{S}_{yy}(\omega)$ is the PSD matrix. In Step 3, the PSD matrix by using the singular value decomposition (SVD) algorithm as follows

$$\boldsymbol{S}_{yy}(\omega) = \boldsymbol{U}(\omega)^T \sum(\omega) \boldsymbol{V}(\omega) \quad (4)$$

where $\sum(\omega)$ is a diagonal matrix containing the singular values $\sigma_i(\omega)$ (i = 1, 2, … n) of its PSD matrices, $\mathbf{U}(\omega)$ and $\mathbf{V}(\omega)$ are unitary matrices. The $\mathbf{U}(\omega)$ matrix equals the $\mathbf{V}(\omega)$ matrix since $\boldsymbol{S}_{yy}(\omega)$ is symmetric. In Step 4, peak frequencies (i.e., natural frequency ω_n) are identified in the first singular value $\sigma_i(\omega)$. In Step 5, the mode shapes are extracted from any of column vectors of $\boldsymbol{U}(\omega)$ at the corresponding peak frequencies (Brinker *et al.* 2000, Yi and Yun 2004).

2.2.2 Stochastic subspace identification method

Brinker and Andersen (2006) state that the stochastic subspace identification (SSI) method is a strong modal analysis technique in the time domain and it involves several difficult mathematic steps. The SSI method is summarized in five steps based on existing studies (Lee *et al.* 2018).

In Step 1, the cross-correlation matrices are calculated from the measured time signals. In Step 2, the Hankel matrix [$\mathbf{H}$] is constructed from the obtained correlation matrices. In Step 3, the invertible weighting matrices $\mathbf{W}_1$ and $\mathbf{W}_2$ are pre- and post-multiplied to the Hankel matrix. Then, this matrix is decomposed into the observability $\boldsymbol{\mathcal{O}}_{n1}$ and the system matrix $\mathbf{A}$ as Eq. (5).

$$\begin{aligned} \mathbf{W}_1\mathbf{H}\mathbf{W}_2 = \ [\mathbf{U}_1 \ \ \mathbf{U}_2] \begin{bmatrix} \boldsymbol{\Sigma}_1 & \mathbf{0} \\ \mathbf{0} & \mathbf{0} \end{bmatrix} \begin{bmatrix} \mathbf{V}_1^{\mathbf{T}} \\ \mathbf{V}_2^{\mathbf{T}} \end{bmatrix} \\ \approx \ \mathbf{U}_1\boldsymbol{\Sigma}_1\mathbf{V}_1^{\mathbf{T}} \Leftrightarrow \ \mathbf{W}_1 \ \mathcal{O}_{\mathrm{n}1}\mathcal{O}_{\mathrm{n}2}\mathbf{W}_2 \end{aligned} \quad (5)$$

The $\mathbf{U}$, $\mathbf{V}$ and $\sum_1$ are the unitary matrices and the singular value matrix respectively. The system matrix $\mathbf{A}$ is obtained from the observability matrix $\boldsymbol{\mathcal{O}}_{n1}$. In Step 4, the eigenvalues μ and the eigenvectors ψ of the system are computed by decomposing the system matrix A as Eq. (6).

$$\begin{gathered} \mathbf{A\Psi} = \mathbf{\Psi M} \\ (\mathbf{M} = \mathrm{diag}(\mu_1, \mu_2, \dots, \mu_N) \ \in \ \mathbf{R}^{N\times N}, \\ \mathbf{\Psi} = [\psi_1, \psi_2, \dots, \psi_N] \ \in \ \mathbf{R}^{N\times N}) \end{gathered} \quad (6)$$

In Step 5, several criteria are applied to classify stable modes, unstable modes and noise modes. Then a proper system order is decided via the Stabilization chart (Yi and Yun. 2004, Brinker and Andersen 2006).

3. Numerical modelling of wind turbine tower with caisson foundation

3.1 Description of target structure

A 3.0 MW offshore wind turbine with a caisson foundation was selected as the target structure for the numerical modeling, as illustrated in Fig. 1. The target structure was assumed to be partially submerged into the ocean with the still water level of 13.69 m, see Fig. 1(a). The geometry of wind turbine tower was based on Hankyung II Wind Park located in Jeju Island, Korea where many onshore and offshore wind turbine towers were installed due to a high potential source of wind energy (Kim *et al.* 2014, Nguyen *et al.* 2015).

The wind turbine has three blades upwind direction with a diameter of 90 m. The nacelle and rotor weigh 68 and 39.8 tons respectively. The tower structure was designed as a steel tube structure, which has a total height of 77.3 m. The cross-sectional thickness of the tower is outlined in Table 1. The tower was assembled from three main segments (a segment of 19.3 m and two segments of 29 m) by using four connection flanges. The top diameter was 2.316 m and the bottom diameter was 4.150 m. Each main segment was formed by several sections with thickness changing along with the elevation.

As shown in Fig. 1(b), the caisson foundation of the offshore wind turbine was selected as a concrete caisson structure with infill sand. The geometry of the caisson foundation was roughly scaled down with a factor of 0.75 from an example design of Daewoo E&C offshore wind turbine supporting structure (Daewoo E&C 2017). The foundation consisted of a tube part (a length of 17.3 m, a diameter of 4.15 m and a thickness of 0.5 m) and a conical part (a length of 17.25 m, a bottom diameter of 11.5 m, a wall thickness of 0.5 m, and a slab thickness of 1.4 m). On the top of the tube part, an anchor (a height of 1.2 m and a thickness of 0.95 m) was designed to connect the foundation with the tower, see Fig. 1(b). Between two the tube and conical parts, there was a stiffener (a height of 0.75 m and a thickness of 0.75 m).

As shown in Fig. 1(c), the geometry of the foundation bed was primarily based on an example of foundation bed for Thornton Bank Offshore Wind Farm (Peire *et al.* 2008, Menge *et al.* 2008, Alonso 2013). The foundation bed was composed of four layers, namely scour protection, backfill, gravel and filter layers. The foundation bed was assumed to be supported by the natural ground of 13 m thick. The diameter of the foundation bed was assumed to be 92 m (i.e., four times the bottom diameter of the conical part of the caisson foundation). The assumptions were based on the criteria to reduce the cost of computation during simulations. As illustrated in Fig. 1(c), the thickness of the scour protection layer and the backfill layer were 1.3 m and 6.3 m respectively; the gravel and filter layers were altogether 2 m thick. The foundation bed was assumed to be supported by the natural ground of 13 m thick. The material properties of the wind turbine tower, the caisson foundation, the foundation bed and the natural ground are listed in Table 2.

3.2 Finite element model of target structure

As shown in Fig. 2(a), the wind turbine tower was modeled by shell elements with thickness varying from 40

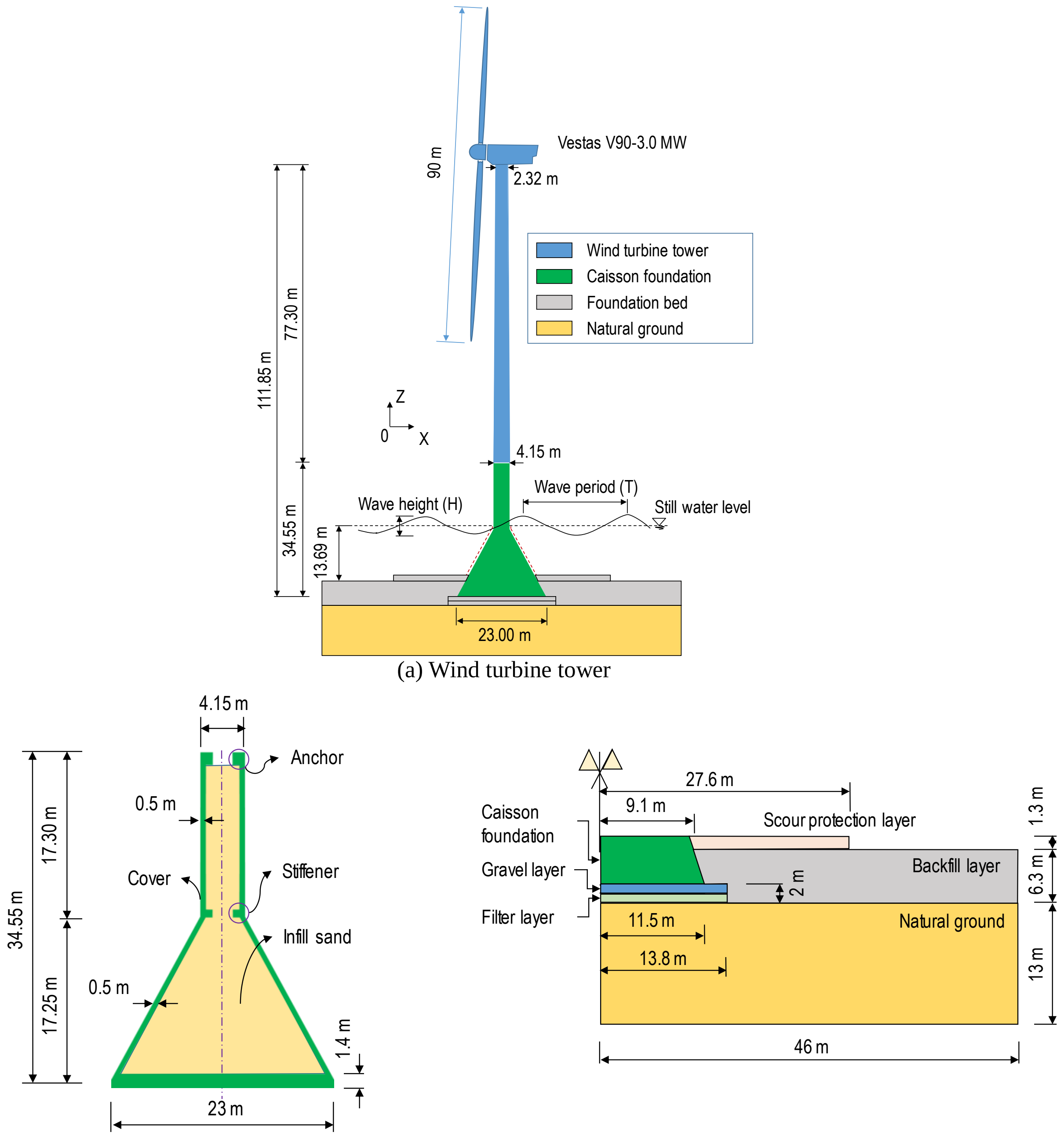

(a) Wind turbine tower

(b) Caisson foundation (c) Foundation bed

Fig. 1 Geometry of wind turbine tower with caisson foundation

Table 1 Cross-sectional thickness of wind turbine tower (Nguyen *et al*. 2015)

Height (m)	Thickness (mm)	Height (m)	Thickness (mm)
0~5.4	40	42.2~50.9	21
5.4~21.9	26	50.9~53.8	19
21.9~30.6	24	53.8~56.7	18
30.6~36.4	23	56.7~59.6	17
36.4~42.2	22	59.6~77.3	16

Table 2 Material properties of wind turbine tower with caisson foundation

Structural Component	Material Type	Modulus of elasticity, E (MPa)	Poisson's ratio, υ	Mass density, ρ (kg/m^3)
Wind turbine tower [a]	Steel	2.10E+05	0.3	7698
Caisson foundation [b]	Concrete	3.35E+04	0.2	2500
	Infill sand	66.5	0.325	1620
Foundation bed [c]	Scour protection layer	-	-	1800
	Backfill layer	66.5	0.325	1620
	Gravel layer	140	0.3	1500
	Filter layer	140	0.3	2100
Natural ground [c]	Sand layer	66.5	0.325	1620

[a] Nguyen *et al.* (2015), [b] Daewoo E&C (2017), [c] Lee *et al.* (2018)

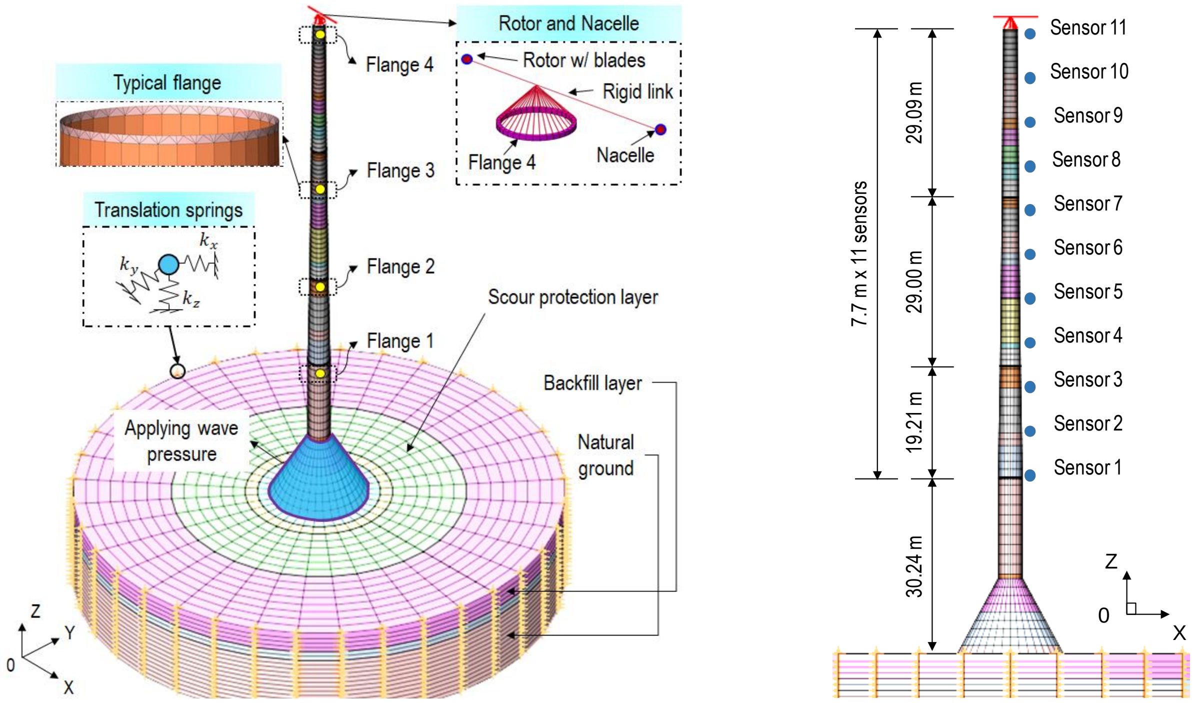

(a) FE model (b) Sensor location

Fig. 2 FE model of wind turbine tower with caisson foundation

mm to 16 mm. At any section, there were 36 elements along the perimeter to maintain continuity in the FE model. The height of a shell element was selected as five times of its width. The four flanges, which were used to connect the main segments of the tower, were also simulated by shell elements. On the top of the model, the rotor with blades and the nacelle were simplified as lump masses. These masses were linked rigidly to the top connection flange of the tower. A part of the caisson foundation was exposed to the sea water since it was inserted into the backfill layer as described in Fig. 1(a).

The caisson foundation was modeled using shell elements for the cover and solid elements for the infill sand. To simulate the submerged condition of the caisson foundation, the effective mass of seawater M_w was considered in the FE model. The added mass of seawater was calculated based on the Westergaard's equation of hydrodynamic water pressure (Lee *et al.* 2012). There were 36 vertical planes in the model. In each plane, the added masses were calculated via integration along the elevation. The width of each plane on each elevation was the width of the element. In the Eq. (7) M_w is the hydrodynamic mass, ρ_w is the seawater density as 1027 kg/m^3, H_w and h are the depth from the water level to the foundation and the water level to the action point of hydrodynamic pressure, respectively.

$$M_w = \int_{h_1}^{h_2} \frac{7}{8} \rho_w \sqrt{H_w h}\ dh \tag{7}$$

All layers of the foundation bed and the natural ground were simulated using solid elements except for the scour protection layer, which was considered as added masses to the foundation bed. To represent the remainder of the natural ground, translation springs in X, Y, Z directions

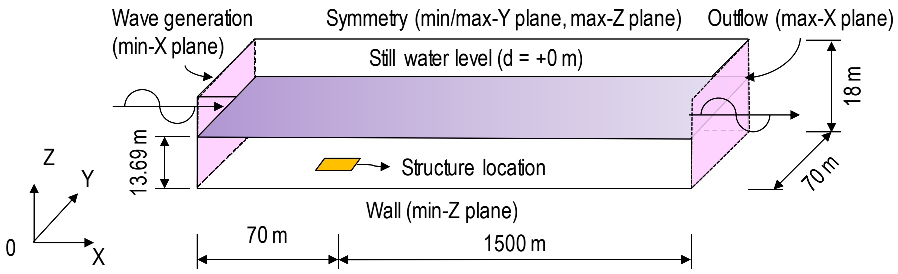

Fig. 3 Numerical modeling of the wave field in Flow-3D

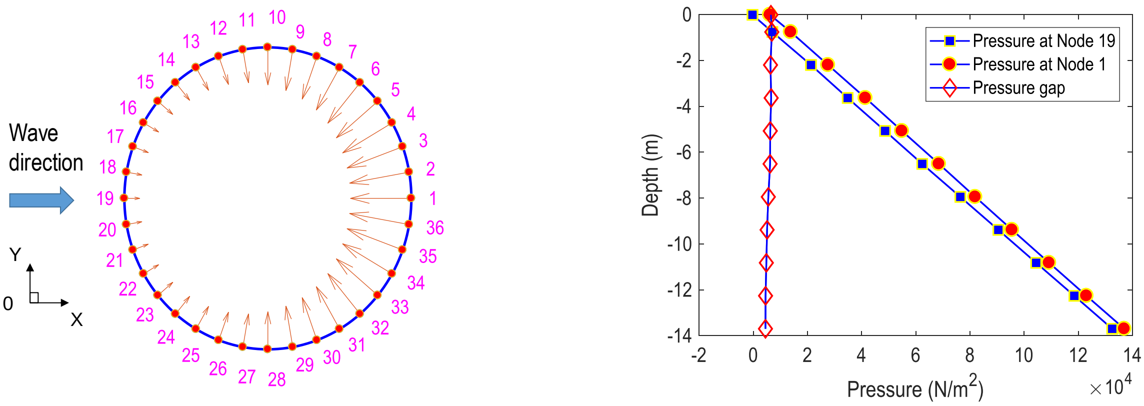

(a) Wave pressure at depth d = -2.2 m

(b) Wave pressure vs depth

Fig. 4 Wave pressure on caisson foundation at t = 0.9 s under Wave 2

Table 3 Wave properties for numerical modeling

Cases	Observation time	Type	Wave height (m)	Wave period (s)
Wave 1	1st Jan 2017	Significant	0.5	6
Wave 2	3rd quarter of 2017	Significant	1.34	6.1
Wave 3	5th Jan 2017	Max	2.8	5.5
Wave 4	9th Jan 2017	Max	4.6	6.5

were assigned to the nodes of the bottom and the surrounding surfaces of the FE model. The spring stiffness of each node was computed as multiplication of the elastic equivalent coefficient and the area supported by the node. For sand, the elastic compressive coefficient C_z is from 5 to 10 kg/cm^2 and the elastic shear coefficient $C_{x,y}$ is about half of C_z (Barkan 1962). To compute the spring stiffness, C_z=7.5 kg/cm/cm^2 and $C_{x,y}$=3.75 kg/cm/cm^2 were selected.

As shown in Fig. 2(b), the acceleration responses of target structure due to wave-induced vibration were extracted by using an array of pseudo sensors, which were equally distributed along the tower.

4. Numerical modelling of wave-induced vibration response

4.1 Simulation of wave pressure on caisson-foundation

As schematized in Fig. 3, the wave field has the following dimensions: 1500 m in length, 70 m in width, and 18 m in height. The incident wave propagated in the X direction, and the caisson foundation was located at 70 m far from the wave generation source. The dimensions of the wave field were determined so that the influence of reflecting waves could be minimized. Regarding the boundary condition, the min-X plane was the plane of wave generation while the max-X plane was the outflow of the domain. The min-Z plane was set to be a wall as the representation of the seabed. The remaining planes were defined as symmetry condition, as shown in Fig. 3. As listed in Table 3, the wave data observed at 32°N-127°E near Jeju Island (Korea) was used as an input for the wave field (Korean Hydrographic and Oceanographic Agency 2017). The selected wave height ranges from 0.5 m to 4.6 m while the selected wave period ranges from 5.5 s to 6.5 s.

For the case of Wave 2, the trend of wave pressure around the caisson foundation at t = 0.9 s is shown in Fig. 4(a).

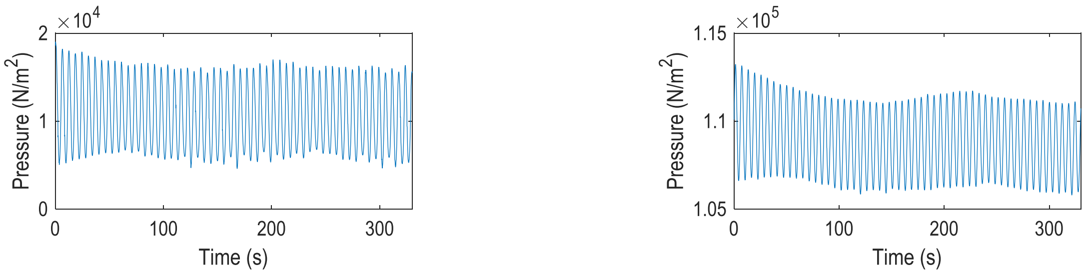

(a) Depth d = -2.2dm (b) Depth d = -11.2dm

Fig. 5 Wave pressure on caisson foundation at Node 1 under Wave 2

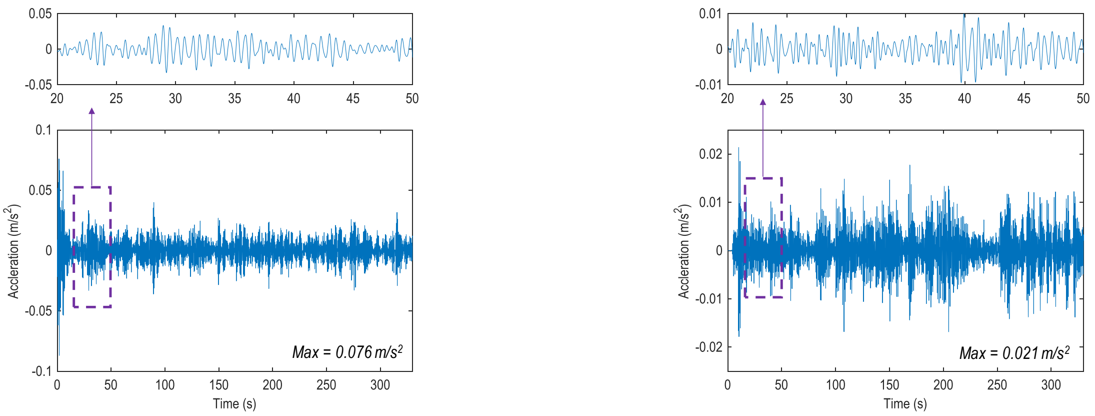

(a) Along-wave directional signal from Sensor 7 (b) Across-wave directional signal from Sensor 7

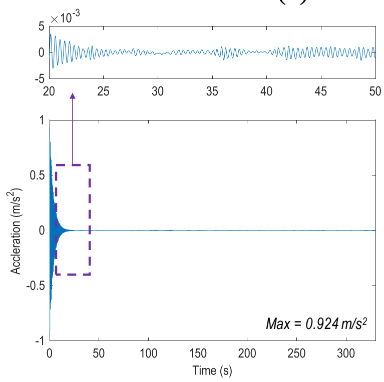

(c) Vertical directional signal from Sensor 7

Fig. 6 Acceleration signals in three directions under Wave 2

In the direction of wave propagation, Node 1 behind the caisson foundation had the largest pressure while Node 19 in front of the caisson foundation had the smallest pressure. The wave pressure at each node also changed with the depth. As shown in Fig. 4(b), wave pressure at Node 1 and Node 19 increased linearly with the depth and the pressure gap between them slightly decreased with the depth (d). Wave pressure on two different depths d = -2.2 m and d = -11.2 m is shown in Figs. 5(a) and 5(b). It is shown that the water pressure at the depth d = -11.2 m had a smaller variation with time as compared to that at the depth d = -2.2 m. This means the deeper depth has a lesser fluctuation of the pressure under the regular wave condition.

4.2 Analysis of wave-induced vibration response

The wave pressure was applied on the caisson foundation, as shown in Fig. 2(a). The measuring period and the sampling rate of acceleration were 330 s and 50 Hz, respectively. Regarding vibration responses, the X, Y and Z directions in the FE model indicates the along-wave direction, the across-wave direction and the vertical direction. With respect to acceleration signals along wave direction, the acceleration from Sensor 11 is the smallest while Sensor 7 has the largest signal. In the vertical accelerations, the largest acceleration signal is from Sensor 1. Due to the similarity of the acceleration signals between sensors, only signal from Sensor 7 in each direction under case of Wave 2 is illustrated as examples in Fig. 6.

Table 4 Max accelerations from Sensor 7 under different waves

Cases	Max value of acceleration (m/s^2)		
	Along-wave direction	Across-wave direction	Vertical direction
Wave 1	0.0152	7.00E-07	0.9064
Wave 2	0.0760	0.0210	0.9240
Wave 3	0.6611	0.1980	0.9034
Wave 4	0.2284	0.1501	1.0038

Table 5 Natural frequencies of free vibration modes

Order	f (Hz)	Description	Order	f (Hz)	Description
1	0.2830	Mode AB1: 1st bending w.r.t X-axis	11	2.4576	Mode CB 4: 4th bending w.r.t Y-axis
2	0.2840	Mode CB1: 1st bending w.r.t Y-axis	12	2.6997	Mode AB5: 5th bending w.r.t X-axis
3	1.5619	Mode AB2: 2nd bending w.r.t X-axis	13	2.7096	Mode CB5: 5th bending w.r.t Y-axis
4	1.5897	Mode CB2: 2nd bending w.r.t Y-axis	14	2.7638	Foundation mode
5	1.8495	Mode AB3: 3rd bending w.r.t X-axis	15	2.7638	Foundation mode
6	1.8820	Mode CB3: 3rd bending w.r.t Y-axis	16	2.9912	Foundation mode
7	2.1152	Mode To1: 1st twisting w.r.t Z-axis	17	2.9912	Foundation mode
8	2.2437	Mode To1: 2nd twisting w.r.t Z-axis	18	3.0270	Mode AB6: 6th bending w.r.t X-axis
9	2.3343	Mode Ax1: 1st elongation w.r.t Z-axis	19	3.0318	Mode Ax1: 2nd elongation w.r.t Z-axis
10	2.4006	Mode AB4: 4th bending w.r.t X-axis	20	3.0437	Mode CB6: 6th bending w.r.t Y-axis

The max value of acceleration signal along-wave direction from Sensor 7 was 0.076 m/s^2 within the first 5 s from the time when the wave approached the caisson foundation as shown in Fig. 6(a). Meanwhile, the maximum value of acceleration signal across-wave direction from Sensor 7 was only 0.021 m/s^2 within the first 10 s, as shown in Fig. 6(b). It is observed in Fig. 6(c) that the vertical acceleration signal from Sensor 7 was similar to a response induced by an impact excitation. This can be explained by the fact that the total vertical force component, which is resulted from the wave pressure, acts similarly as a step force because the mean value of the total vertical force was much larger than the variation. It is rooted from the fact that the wave pressure is always perpendicular to the caisson foundation surface. Meanwhile, in the along or across-wave direction, the variation of the total force component was comparable with its mean value; hence these components act similarly as harmonic forces. This explains why this phenomenon did not happen in the vibration response along and across-wave directions.

The max values of the acceleration signals from Sensor 7 in each direction under other wave conditions are illustrated as shown in Table 4. The max values tended to increase from the case of Wave 1 to the case of Wave 3 in the along and across-wave directions.

5. Vibration characteristics of wind turbine tower with caisson foundation

5.1 Free vibration analysis

The vibration characteristics of the GBF WTT were analyzed by free vibration analysis. The analysis shows that the vibration responses of the GBF WTT included the motions of the tower and the foundation. Lee *et al.* (2018) were also found the similar modes which have combined motions of gravity-type caisson and foundation from the simulations of caisson-foundation breakwater system. In the first 20 modes, 16 tower's motions and 4 foundation motions were found. Natural frequencies of the free vibration modes were summarized in Table 5. The tower's motion can be classified as bending modes with respect to X-axis or Y-axis, elongation modes with respect to Z-axis, twisting modes with respect to Z-axis. The foundation vibrates only in case of the foundation's motion. In this paper, the foundation's motion was not considered since the foundation's motion can't be identified in real experimental condition.

5.1.1 Along-wave directional bending modes

The first four along-wave directional bending modes (i.e., bending with respect to X-axis) of the GBF WTT are presented in Fig. 7 and Table 5. Mode AB1 was found at 0.2830 Hz, which was significantly lower than the natural frequency in Mode AB2 at 1.5619 Hz. Mode AB3 and Mode AB4 were observed at 1.8495 Hz and 2.4006 Hz, respectively. In Mode AB1, the largest vibration area was at the top of the wind turbine tower. Meanwhile, the area in two-third elevation of wind turbine tower had the largest modal amplitude among other three modes. The mode shape amplitude reduced when the elevation came down due to an increase of structural stiffness. In the foundation bed, the areas under two sides of caisson foundation along-wave direction vibrated comparatively larger than other parts. It is noted that the last three mode shapes were similar to Mode AB2 due to the effect of foundation vibration.

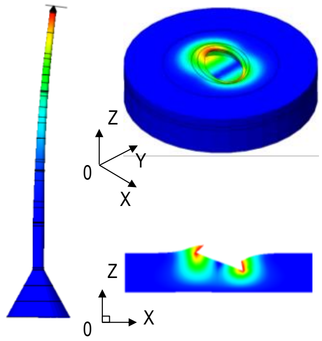

(a) Mode AB1 (0.2830 Hz)

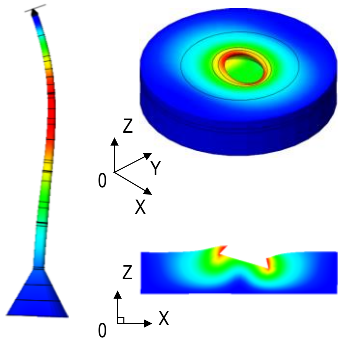

(b) Mode AB2 (1.5619 Hz)

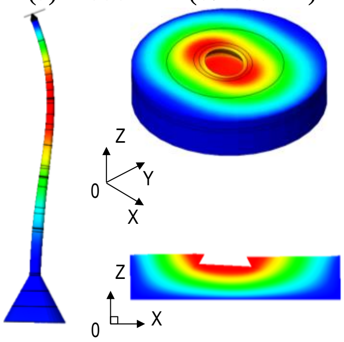

(c) Mode AB3 (1.8495 Hz)

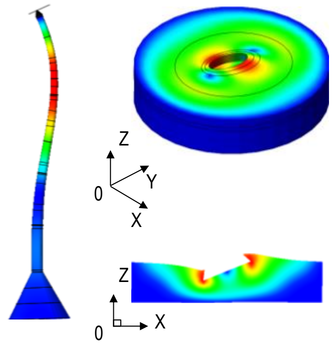

(d) Mode AB4 (2.4006 Hz)

Fig. 7 Along-wave directional bending modes of the GBF WTT

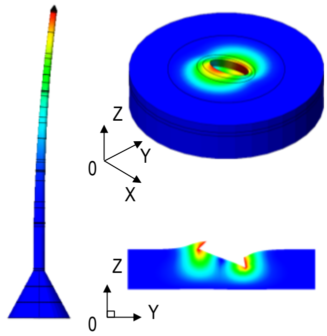

(a) Mode CB1 (0.2840 Hz)

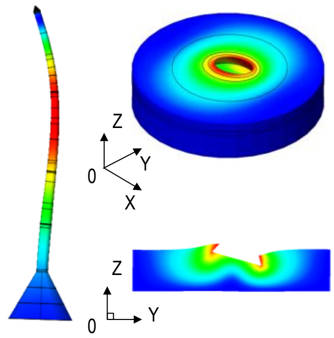

(b) Mode CB2 (1.5897 Hz)

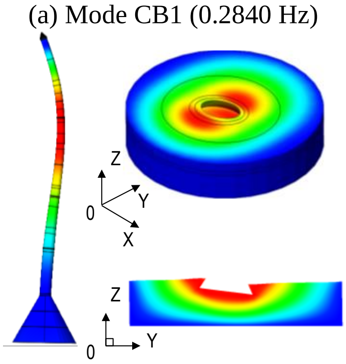

(c) Mode CB3 (1.8820 Hz)

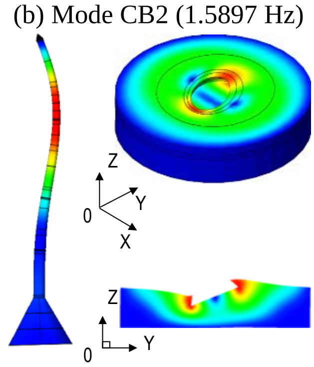

(d) Mode CB4 (2.4576 Hz)

Fig. 8 Across-wave directional bending modes of the GBF WTT

(a) Mode Ax1 (2.3343 Hz) (b) Mode Ax2 (3.0318)

Fig. 9 Axial modes of the GBF WTT

(a) Mode To1 (2.1152 Hz) (b) Mode To2 (2.2437 Hz)

Fig. 10 Torsional modes of the GBF WTT

5.1.2 Across-wave directional bending modes

The first four across-wave directional bending modes (i.e., bending with respect to Y-axis) of the GBF WTT are shown in Fig. 8 and Table 5. Mode CB1 was found at 0.2840 Hz, which was significantly lower than the natural frequency in Mode CB2 at 1.5897 Hz. Mode CB3 and Mode CB4 were observed at 1.8820 Hz and 2.4576 Hz, respectively. It is noteworthy that the natural frequency from the across-wave direction in each mode was higher than that from the along-wave direction. The first four mode shapes of the target structure were similar to those from the along-wave direction. It is observed that the mode shapes from Mode CB2 to Mode CB4 were similar due to the effect of foundation vibration.

5.1.3 Axial and torsional modes

The first two axial modes of the GBF WTT (i.e., elongation with respect to Z-axis) are shown in Fig. 9 and Table 5. The natural frequencies of these modes were at 2.3343 Hz and 3.0318 Hz, respectively. The first two torsional modes (i.e., twisting with respect to Z-axis) of the target structure are shown in Fig. 10 and Table 5. The natural frequencies of the torsional modes were found at 2.1152 Hz and 2.2437 Hz, respectively. In both axial and torsional modes, the foundation bed also vibrated along upper parts, and modal amplitudes increased along the elevation of the tower.

5.2 Wave-induced forced vibration analysis

The wave-induced forced vibration analysis was employed by using the acceleration signals of the target structure under the case of Wave 2. Regarding the acceleration signals, the sampling frequency was f_s = 50 Hz and the measuring period was T = 330 s, hence the Nyquist frequency was 25 Hz. In all forced vibration modes, the FDD method (resolution 0.012 Hz) was first employed by using accelerations from Sensor 1 and 11, and then the combined FDD and SSI methods (resolution 0.006 Hz) were utilized by using accelerations from all sensors to identify reliable modal parameters. In the combined FDD and SSI method, modes were identified from overlapped chart of the singular values in FDD method and stabilization chart in SSI method. Then, the modal parameters were extracted from the SSI method for the identified modes.

5.2.1 Along-wave directional bending modes

As shown in Figs. 11(a) and 11(b), it is noted that Mode AB1 was not clearly identified via using acceleration signal from Sensor 1, while it was successfully identified via using acceleration signal from Sensor 11. The natural frequencies from Sensor 1 and Sensor 11 were matched altogether. As shown in Fig. 11(c), the first peak at 0.1634 Hz resulted from the incident wave (i.e., Wave 2 with the significant

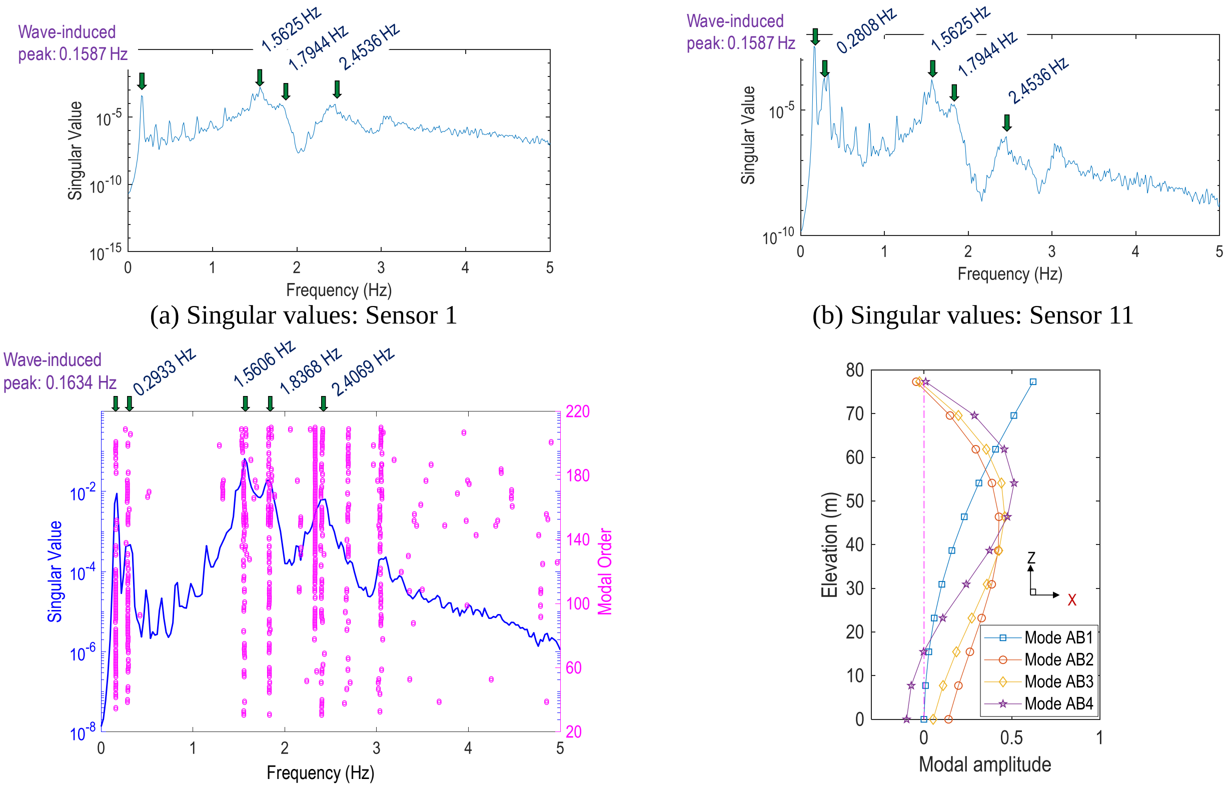

(a) Singular values: Sensor 1 (b) Singular values: Sensor 11

(c) Combined FDD and SSI methods (d) Mode shapes

Fig. 11 Modal parameter identification for along-wave directional bending modes

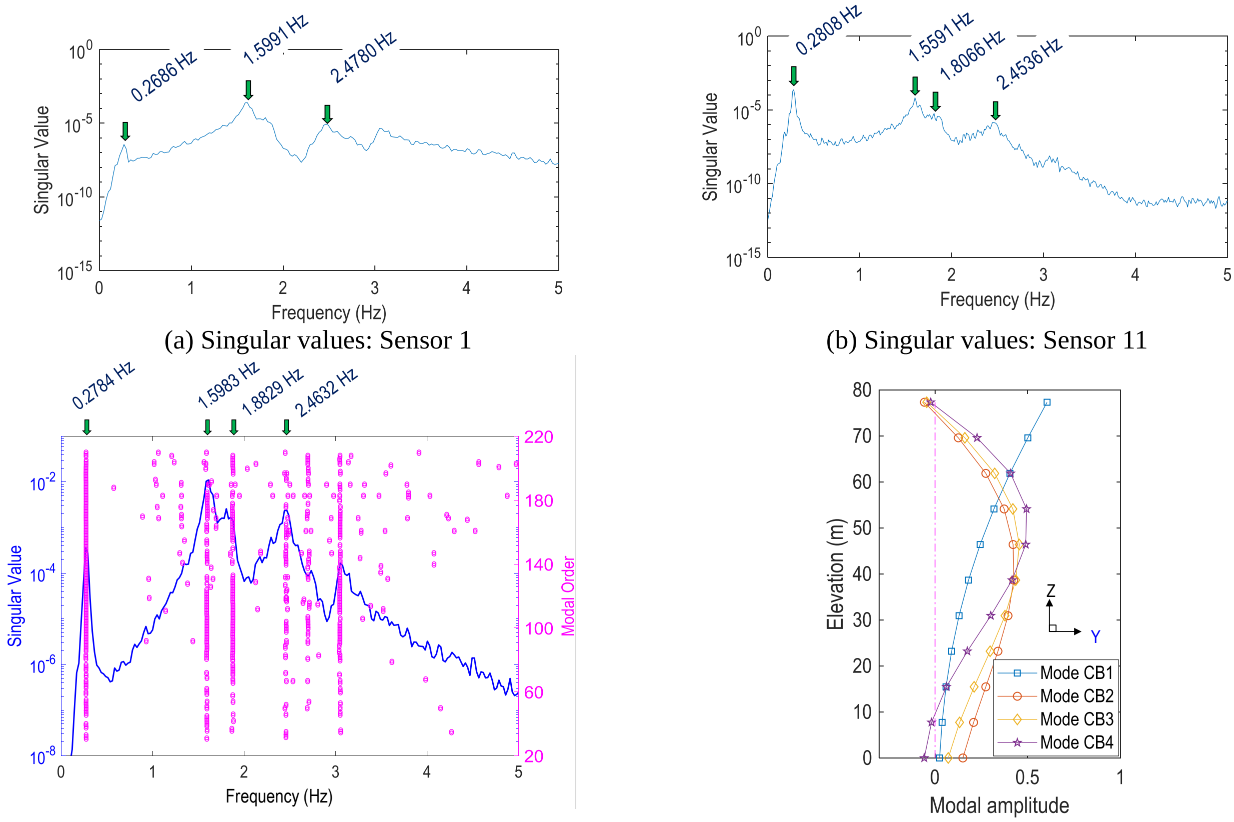

(a) Singular values: Sensor 1 (b) Singular values: Sensor 11

(c) Combined FDD and SSI methods (d) Mode shapes

Fig. 12 Modal parameter identification for across-wave bending modes

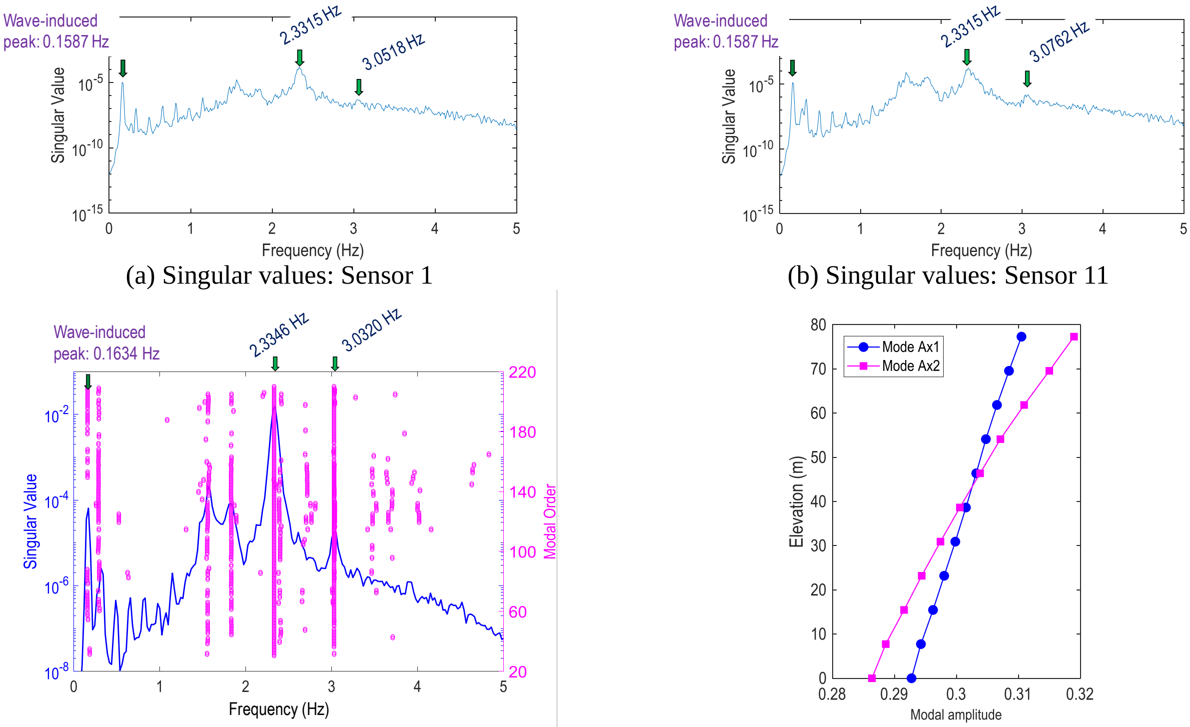

(a) Singular values: Sensor 1 (b) Singular values: Sensor 11

(c) Combined FDD and SSI methods (d) Mode shapes

Fig. 13 Modal parameter identification for axial modes

wave period T_s = 6.1 s). Likewise, this phenomenon was also observed in other small aliasing peaks, which were not structural natural frequencies.

From Fig. 11(c), the first four along-wave directional bending modes of the GBF WTT were identified: Mode AB1 at 0.2933 Hz, Mode AB2 at 1.5606 Hz, Mode AB3 at 1.8368 Hz and Mode AB4 at 2.4069 Hz. These extracted natural frequencies matched with those from the free vibration analysis under 4%, as shown in Table 6. It is observed that the difference between the free vibration and forced vibration analyses was largest for Mode AB1. As shown in Fig. 11(d), the corresponding mode shapes were similar to those from the free vibration analysis.

5.2.2 Across-wave directional bending modes

As shown in Figs. 12(a) and 12(b), it is noted Mode CB3 was not identified via using acceleration signal from Sensor 1, while it was successfully identified via using acceleration signal from Sensor 11. As shown in Fig. 12(c), it is noted that there was an absence of the first aliasing peak rooted from the significant wave period.

From Fig. 12(c), the first four across-wave directional bending modes of the GBF WTT were identified: Mode CB1 at 0.2784 Hz, Mode CB2 at 1.5983 Hz, Mode CB3 at 1.8829 Hz and Mode CB4 at 2.4632 Hz. These extracted natural frequencies matched with those from the free vibration analysis under 3% difference, as shown in Table 7. The gap between natural frequencies from the free vibration and forced vibration analyses was largest for Mode CB1. As shown in Fig. 12(d), the corresponding mode shapes were similar to those from the free vibration analysis.

5.2.3 Axial and torsional modes

As shown in Figs. 13(a) and 13(b), the natural frequencies from Sensor 1 and Sensor 11 were similar in each mode. As shown in Fig. 13(c), the first peak at 0.1634 Hz resulted from the significant wave period.

There were several notable peaks which could be combination peaks from bending modes in the along and across-wave directions, and these peaks did not belong to axial modes. From Fig. 13(c), the first two axial modes of the GBF WTT were identified: Mode Ax1 at 2.3346 Hz and Mode Ax2 at 3.0320 Hz.

Table 6 Natural frequencies of along-wave directional bending modes

Analysis	Mode AB1	Mode AB2	Mode AB3	Mode AB4
Free vibration	0.2830 Hz	1.5619 Hz	1.8495 Hz	2.4006 Hz
Forced vibration	0.2933 Hz	1.5606 Hz	1.8368 Hz	2.4069 Hz
Difference	3.51 %	0.08 %	0.69 %	0.26 %

Table 7 Natural frequencies of across-wave bending modes

Analysis	Mode CB1	Mode CB2	Mode CB3	Mode CB4
Free vibration	0.2840 Hz	1.5897 Hz	1.8820 Hz	2.4576 Hz
Forced vibration	0.2784 Hz	1.5983 Hz	1.8829 Hz	2.4632 Hz
Difference	2.01 %	0.54 %	0.05 %	0.23 %

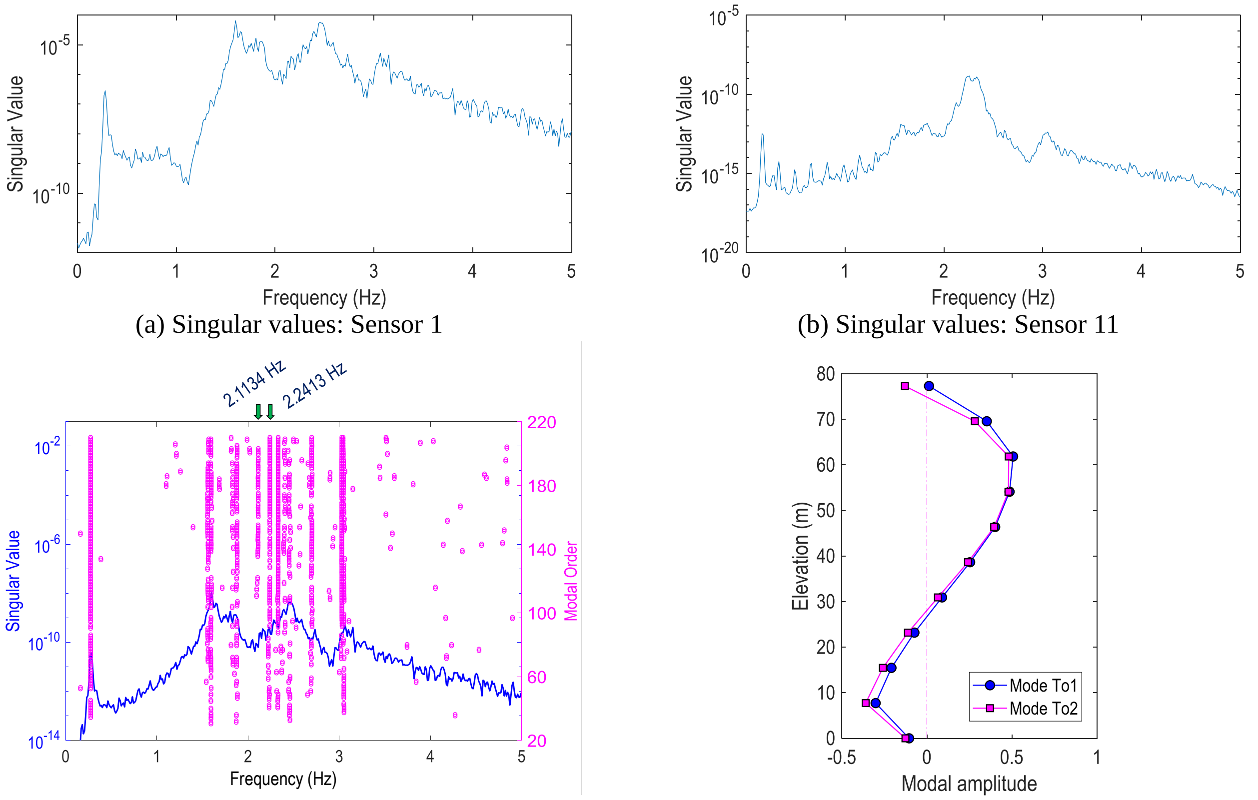

(a) Singular values: Sensor 1
(b) Singular values: Sensor 11
(c) Combined FDD and SSI methods
(d) Mode shapes

Fig. 14 Modal parameter identification for torsional modes

The identified natural frequencies of the axial modes matched the values from the free vibration analysis, as shown in Table 8.

The corresponding mode shapes were also similar to those from the free vibration analysis, as shown in Fig. 13(d). It is observed that the modal value increased nearly linearly along with elevation.

As shown in Figs. 14 (a) and 14(b), the SVD charts of FDD method using acceleration from vertical rotation of motion contain many peaks, which could be combination peaks from bending modes in the along and across-wave directions, and these peaks did not belong to the torsional modes. From Fig. 14(c), the first two torsional modes were identified: Mode To1 at 2.1134 Hz and Mode To2 at 2.2413 Hz. The identified natural frequencies matched the values from the free vibration analysis, as shown in Table 9. The

torsional mode shapes were also similar to those from bending mode shapes, as shown in Fig. 14(d). They were different from the mode shapes from the free vibration analysis in which modal amplitudes increased along with the elevation in both modes. This can be due to the extraction of the modal amplitude of vertical rotation between different analyses.

Conclusively, the bending modes, axial and torsional modes were successfully identified via several accelerometers, and the structural vibration response contained a property of the incident wave.

Table 8 Natural frequencies of axial modes

Analysis	Mode Ax1	Mode Ax2
Free vibration	2.3343 Hz	3.0318 Hz
Forced vibration	2.3346 Hz	3.0320 Hz
Difference	0.01%	0.00%

Table 9 Natural frequencies of torsional modes

Analysis	Mode To1	Mode To2
Free vibration	2.1152 Hz	2.2437 Hz
Forced vibration	2.1134 Hz	2.2413 Hz
Difference	0.09 %	0.11%

5.3 Modal parameter extraction under different wave conditions

To obtain reliable results of output-only modal identification, vibration responses of the GBF WTT should be measured under proper wave conditions. In this section, the effect of wave height and wave period on the mode identification was investigated four different wave conditions (i.e., Waves 1–4), as described in Table 3. The natural frequencies and mode shapes of bending modes were compared between the free vibration and the wave-induced forced vibration analyses by employing the relative variation of natural frequency and the modal assurance criterion (MAC), respectively.

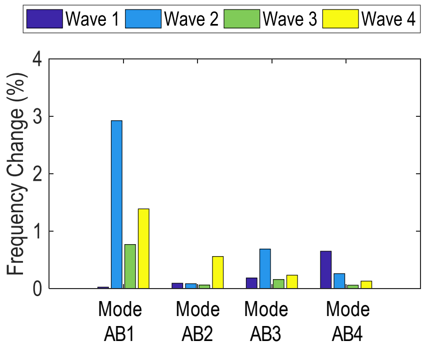

(a) Along-wave direction

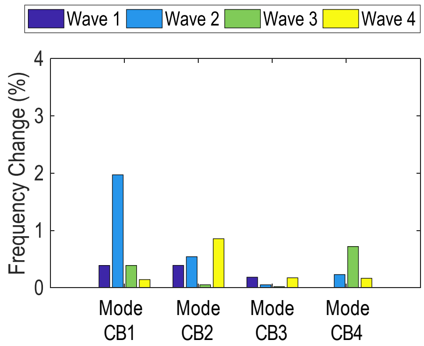

(b) Across-wave direction

Fig. 15 Comparison of natural frequencies: free vibration and wave-induced forced vibration analyses

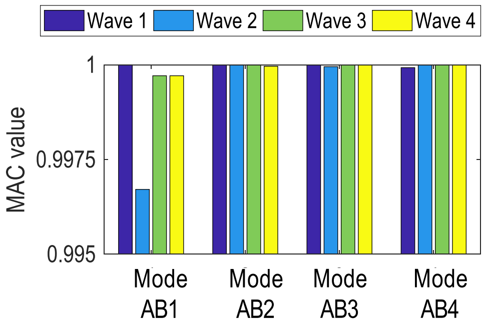

(a) Along-wave direction

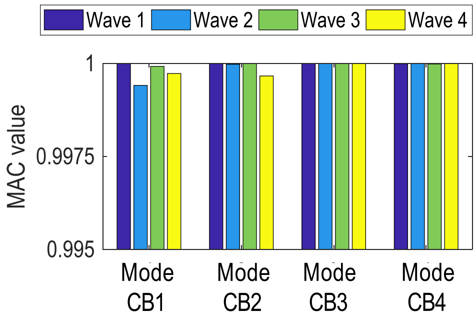

(b) Across-wave direction

Fig. 16 Comparison of mode shapes: free vibration and wave-induced forced vibration analyses

The relative variation between natural frequencies from the free vibration and the forced vibration analyses were calculated as Eq. (8). In this equation, f_{fr} and f_{fo} are the natural frequencies from the free vibration and forced vibration analyses.

$$MAC\ (\Phi_i, \Phi_i^*) = \frac{[\Phi_i^T \Phi_i^*]^2}{[\Phi_i^T \Phi_i\ ][\Phi_i^{*T} \Phi_i^*]} \tag{9}$$

As shown in Fig. 15, the first natural frequency of bending modes in both directions varied largely compared to remaining ones because the frequencies of incident waves were similar to the first natural frequency of bending modes. Natural frequencies in three remaining modes in both directions were less likely to change under various wave conditions (variation under 1%). Regarding mode shape, it is observed that all cases in both directions had the MAC value over 0.99, as shown in Fig. 16. It means that these corresponding mode shapes from wave-induced forced vibration analyses highly matched with those from the free vibration analyses. However, the mode shape of Mode 1 was likely to change with the variation of wave conditions. From the above observation, it is recognized that when the frequency of the wave was near the structural natural frequency, it has an influence on the modal parameters of that mode. This led to a situation that structural damages could be hidden from the variation of coming waves in the field.

6. Conclusions

In this study, vibration characteristics of offshore wind turbine tower (WTT) with gravity-based foundation (GBF) were identified from dynamic responses under wave-induced excitations. The following approaches are implemented to achieve the objective. Firstly, the operational modal analysis methods such as frequency domain decomposition (FDD) and stochastic subspace identification (SSI) were selected to estimate modal parameters from output-only dynamic responses. Secondly, a GBF WTT model composed of superstructure, substructure and foundation was simulated as a case study by using a structural analysis program, MIDAS FEA. Thirdly, wave pressures acting on the WTT structure are established by nonlinear regular waves which were simulated from a computational fluid software, Flow 3D. Wave-induced acceleration responses of the target structure were analyzed by applying the simulated wave pressures to the GBF WTT model. Finally, modal parameters such as natural frequencies and mode shapes were estimated from the output-only acceleration responses and compared with the results obtained from the free vibration analysis. The effect of wave height and period on modal parameter extraction was also investigated for the mode identification of the GBF WTT.

From the numerical investigation, at least three concluding remarks can be made, as follows:

(1) The vibration of the foundation bed had an influence on the mode shape of the target structure.
(2) The vibration responses of the wind turbine tower with caisson foundation reflected not only the structural behaviours but also the property of the incident wave. The bending modes and the axial modes of the target structure could be identified successfully via the acceleration responses of the structure under wave excitation.
(3) When the frequency of incident wave was similar to the fundamental frequency of the target structure, the damage-induced frequency variation could be overshadowed by the wave-induced frequency variation.

The experimental examination of a real wind turbine tower with caisson foundation under not only various waves but also wind and earthquake conditions remains as future work. The effect of foundation bed size on the structural modal parameters should be also investigated.

Acknowledgments

This work was supported by the National Research Foundation of Korea (NRF) grant funded by the Korea government (MSIT) (NRF-2018R1A6A3A01013004).

References

4Coffshore (2018), https://www.4coffshore.com/windfarms/gravity-based-support-structures-aid8.html, 2018.12.31.

Banerjee, A., Chakraborty, T. and Matsagar, V. (2018), "Dynamic analysis of an offshore wind turbine considering frequency-dependent soil–structure interaction parameters", *Int. J. Struct. Stab. Dynam.*, **18**(6), 1850086. https://doi.org/10.1142/S0219455418500864.

Barkan, D.D. (1962), "Dynamics of bases and foundations", *McGraw-Hill Book Co.*, New York, USA.

Brinker, R. and Andersen, P. (2006), "Understanding stochastic subspace identification", *Proceedings of the 24th International Modal analysis Conference*, St. Louis, Missouri.

Brinker, R., Zhang, L. and Andersen, P. (2001), "Modal identification of output-only systems using frequency domain decomposition", *Smart Mater. Struct.*, **10**, 441-445.

Chong, N. and Li, R. (2016), Offshore Wind Farms: Technologies, Design and Operation, *Woodhead Publishing*, DOI: 10.1016/C2014-0-00763-0.

Daewoo E&C (2017), "Offshore Wind Concrete Gravity Based Substructure-Design and Construction Guidelines", *Daewoo Institute of Construction Technology*, Korea.

Damgaard, M. (2014), "Dynamic properties of offshore wind turbine foundations", PhD thesis, Aalborg University, Nov. 2014.

Esteban, M.D., Counage, B., Lopez-Gutierrez, J.S., Negro, V. and Vellisco, F. (2015), "Gravity based support structures for offshore wind turbine generators: Review of the installation process", *Ocean Eng.*, **110**, 281-291. https://doi.org/10.1016/j.oceaneng.2015.10.033.

Ewins, D.J. (2000), "Modal Testing: theory, practice and application, 2nd edition", *Research Studies Press Ltd.*, Hertfordshire, UK.

Huynh, T.C., Lee, S.Y., Dang, N.L. and Kim, J.T. (2018), "Vibration-based structural identification of caisson-foundation system using in situ measurement and simplified model", *Struct. Control Health Monit.*, Article ID: e2315, DOI: 10.1002/stc.2315.

Kim, T., Baek, S., Park, E. and Chang, H.J. (2014), "Optimal green energy management in Jeju, South Korea: On-grid and off-grid electrification", *Renew. Energ.*, **69**, 123-133. https://doi.org/10.1016/j.renene.2014.03.004.

Korean Hydrographic and Oceanographic Agency. (2017), "Ocean Observation Newsletter – 3rd Quarter 2017", *National Oceanographic Research Institute*, Republic of Korea.

Lee, S.Y. and Kim, J.T. (2015), "Effects of foundation damage and water-level change on vibration modal parameters of gravity-type caisson structure", *Science China Technological Sciences*, **58**(2), 316-329.

Lee, S.Y., Huynh, T.C. and Kim, J.T. (2015), "Structural identification of gravity-type caisson structure via vibration feature analysis", *Smart Struct. Syst.*, **15**(2), 259-281. http://dx.doi.org/10.12989/sss.2015.15.2.259

Lee, S.Y., Huynh, T.C. and Kim, J.T. (2018), "A practical scheme of vibration monitoring and modal analysis for caisson breakwater", *Coast. Eng.*, **137**, 103-119. https://doi.org/10.1016/j.coastaleng.2018.03.008.

Lee, S.Y., Nguyen, K.D., Huynh, T.C., Kim, J.T., Yi, J.H. and Han, S.H. (2012), "Vibration-based damage monitoring of harbor caisson structure with damaged foundation-structure interface", *Smart Struct. Syst.*, **10**(6), 517-547. http://dx.doi.org/10.12989/sss.2012.10.6.517.

Lee, S.Y., T.C., Huynh, Kim, J.T. Yoon, H.S. and Han, S.H. (2013), "Vibration characteristics of gravity-type caisson breakwater structure with water-level variation", *Int. J. Distrib. Sens. N.*, **9**(11), 1-13. https://doi.org/10.1155/2013/261396.

Menge, P. and Gunst, N. (2008), "Gravity base foundation for the wind turbines on the thornton bank-Belgium", *Proceedings of the 15th Innovatieforum Geotechniek*, Antwerpen, Belgium.

MOTIE (2018), Ministry of Trade, Industry and Energy, May 2018.

Nguyen, C.U., Huynh, T.C. and Kim, J.T. (2018), "Vibration-based damage detection in wind turbine towers using artificial neural networks", *Struct. Monit. Maint.*, **5**(4), 507-519. https://doi.org/10.12989/smm.2018.5.4.507.

Nguyen, C.U., Huynh, T.C., Dang, N.L. and Kim, J.T. (2017), "Vibration-based damage alarming criteria for wind turbine towers", *Struct. Monit. Maint.*, **4**(3), 221-236. https://doi.org/10.12989/smm.2017.4.3.221.

Nguyen, T.C., Huynh, T.C. and Kim, J.T. (2015), "Numerical evaluation for vibration-based damage detection in wind turbine tower structure", *Wind Struct.*, **21**(6), 657-675. http://dx.doi.org/10.12989/was.2015.21.6.657.

Nguyen, T.C., Huynh, T.C. and Kim, J.T. (2017), "Hybrid bolt-loosening detection in wind turbine tower structures by vibration and impedance responses", *Wind Struct.*, **24**(4), 385-403. https://doi.org/10.12989/was.2017.24.4.385.

Overschee, V.P. and De Moor, B. (1996), "Subspace identification for linear system", *Kluwer Academic Publisher*, Dordrecht, Netherlands.

Park, J.H. (2009), "Development of Autonomous Smart Sensor Nodes for Hybrid Structural Health Monitoring of Large Structures", Doctoral Thesis, Department of Ocean Engineering, Pukyong National University.

Peire, K., Nonneman and H., Bosschem, E. (2008), "Gravity base foundations for the thornton bank offshore wind farm", *Proceedings of the CEDA*, Antwerp, Belgium.

Petersen, T.U., Sumer, B.M., Fredsoe, J., Raaijmakers, T.C. and Schouten, J.J. (2015), "Edge scour at scour protections around piles in the marine environment – Laboratory and field investigation", *Coast. Eng.*, **106**, 42-72.

https://doi.org/10.1016/j.coastaleng.2015.08.007.

Risi, R.D., Bhattacharya, S. and Goda, K. (2018), "Seismic performance assessment of monopile-supported offshore wind turbines using unscaled natural earthquake records", *Soil Dyn. Earthq. Eng.*, **109**, 154-172. https://doi.org/10.1016/j.soildyn.2018.03.015.

Smaling, H. (2014), Hydrodynamic loading on the shaft of a gravity based offshore wind turbine, *Final Report Master Thesis*, TU Delft, May 2018.

Wang, S., Huang, Y., Li, L., Liu, C. and Zhang, D. (2017), "Dynamic analysis of wind turbines including nacelle-tower-foundation interaction for condition of incomplete structural parameters", *Adv. Mech. Eng.*, **9**(3), 1-17. https://doi.org/10.1177/1687814017692940.

Wang, X., Zeng, X., Li, J., Yang, X. and Wang, H. (2018), "A review on recent advancements of substructures for offshore wind turbines", *Energ. Convers. Manage.*, **158**, 103-119. https://doi.org/10.1016/j.enconman.2017.12.061.

West, W.M. (1984), "Illustration of the Use of Modal Assurance Criterion to Detect Structural Changes in an Orbiter Test Specimen", *Proceedings of the Air Force Conference on Aircraft Structural Integrity*, 1-6.

Wickramasinghe, W.R., Thambiratnam, D.P., Chan, T.H.T. and Nguyen, T. (2016), "Vibration characteristics and damage detection in a suspension bridge", *J. Sound Vib.*, **375**, 254-274. https://doi.org/10.1016/j.jsv.2016.04.025.

Wind EUROPE (2018), Wind in power 2017: Annual combined onshore and offshore wind energy statistics, February 2018, www.windeurope.org.

Yi, J.H., and Yun, C.B. (2004), "Comparative study on modal identification methods using output-only information", *Struct. Eng. Mech.*, **17**(3-4), 445-446. https://doi.org/10.12989/sem.2004.17.3_4.445.

CC